Nigerian Research Journal of Engineering and Environmental Sciences 6(2) 2021 pp. 714-726
p ISSN: 2635-3342; e ISSN: 2635-3350

Nigerian Research Journal of Engineering and Environmental Sciences
Journal homepage: www.rjees.com

Original Research Article

Modelling and Analysis of an Inverter-Start Six-Phase Induction Motor using Finite Element Analysis

***Epemu, A.M. and Nyong-Bassey, B.E.**

Department of Electrical/Electronics Engineering, College of Engineering and Technology, Federal University of Petroleum Resources Effurun, PMB 1221, Effurun, Delta State, Nigeria.
*epemu.ayebatonye@fupre.edu.ng; nyongbassey.bassey@fupre.edu.ng

http://doi.org/10.5281/zenodo.5805310

ARTICLE INFORMATION

Article history:
Received 17 Nov, 2021
Revised 07 Dec, 2021
Accepted 08 Dec, 2021
Available online 30 Dec 2021

Keywords:
Mathematical modelling
Inverter-start
Finite element analysis
Multi-phase induction machines
Distributed windings

ABSTRACT

This paper presents the finite element analysis (FEA) of a six-phase inverter-start induction motor (IM), which has several benefits such as high-fault tolerance, less torque pulsations and high-power output when compared to the conventional three-phase line-start IM. The motor is inverter-start hence the need for a voltage source inverter circuit that will drive the IM. The machine stator windings are distributed windings derived from splitting the stator of a conventional three-phase IM into two, to form a six-phase stator with no displacement angle of the winding sets. The Six-phase inverter-start IM was modelled and simulated using ANSYS electronics desktop finite element analysis (FEA) software. The performance characteristics, such as speed, torque, stator currents, magnetic flux density, and magnetic vector potential were observed and compared to the conventional d-q method. The analysis was seen to provide actual accurate insight into the operation of the six-phase inverter start IM that other numerical methods cannot provide.

1. INTRODUCTION

Electrical machines could be designed as line-start or inverter-start. The advent and constant improvement of power electronics drives have increased the use of inverters to drive multiphase machines (Levi et al., 2007). The induction motor (IM) is the simplest electrical machine in terms of construction. The rotating magnetic field of the rotor cuts the stationary stator, causing an electromagnetic field to be induced into the rotor. The electric current in the rotor required to produce torque in an induction motor is acquired via electromagnetic induction from the stator winding's revolving magnetic field. An induction motor's rotor can be either a squirrel cage rotor or a wound type rotor. Due to simple and durable construction without

mechanical commutators, AC motors are currently chosen over DC motors in most applications. The most often used AC motor for industrial control and automation is the induction motor, which is also known as the workhorse of the motion industry, due to its simple and robust construction, low cost, high efficiency, reasonably good power factor, self-starting, and low maintenance cost as seen in Melfi et al. (2009). The six-phase induction motors are inverter start and are preferable for high power applications than three-phase motors (Khoucha *et al.*, 2009; Liang and Ilochonwu, 2010).

Multiphase induction motors such as five-phase, six-phase and nine-phase induction motors are known to be highly fault-tolerant when compared to the conventional three-phase induction motor. They are also seen to have less torque pulsations and lower harmonic current, hence the recent interest in them, especially in applications where the reliability of the induction motor is of utmost importance (Abbas *et al*., 1984; Loriya and Patel, 2016; Gaikwad and Shinde, 2020). The simulation of inter-turn and phase faults performance analysis of multiphase induction motor was presented by De Rossiter Corrêa *et al.* (2001), while Kammoun *et al.* (2015) showed that inverter start multiphase motors were highly fault-tolerant when compared to their three-phase winding counterpart.

The modelling and simulation of the induction motor was earlier carried as far back as 1965 by Krause and Thomas, (1965), and an investigation of an inverter fed five-phase induction motor was carried out in 1969 by Ward and Härer (1969). A digital simulation of a three-phase induction motor was presented by Ghani, (1988) where he showed the dynamic behaviour of the motor. Multiphase phase induction motors are mostly modelled either in natural machine variables or in d-q variables and simulated using MATLAB/Simulink (Singh *et al*., 2003; Kundrotas *et al*., 2014; Dattu and Rashmi, 2017). The modelling and analysis of the inverter start six-phase induction model have previously been carried out by Ogunjuyigbe *et al.* (2014), the authors modelled the motor in d-q variables and presented a step by step method of simulation in MATLAB/Simulink. Results showed performance characteristics expected, but still does not portray the actual behaviour of the motor since stator slot permeance harmonics, winding harmonics, and the actual air gap function was not taken into consideration. Kaliyavarathan and Sivakumaran, (2020) presented a design and performance analysis of a novel multiphase induction motor with die-cast copper rotors using Finite element analysis (FEA) for electric propulsion vehicles applications. A unique multiphase die-casting induction machine was created in this study. The authors concluded that multiphase die-casting induction motors outperformed other conventional machines. Since the six-phase IM machines were previously modelled in natural machine variables and d-q variables and simulated in MATLAB/Simulink, stator slot permeance harmonics, winding harmonics and actual air gap function were not taken into consideration. Hence, results from such methods are not too accurate. Although the use of FEA is more accurate, this does not in any way invalidate the results from other numerical methods using MATLAB/Simulink. The FEA is perceived to be the most accurate method for the analysis of electrical machines as machine parameters are accurately calculated through the direct calculation of the magnetic field in the machine domain (Epemu *et al.*, 2021).

The purpose of this paper is to model and analyze the six-phase inverter-start IM model using finite element analysis to provide a true insight into the operations of the motor which is more accurate than other numerical methods such as the d-q, natural phase variable method and the complex vector approach.

2. METHODOLOGY

The analysis of the inverter-start six-phase induction motor was done using the d-q method and the finite element analysis approach. The electromagnetic field analysis and the dynamic simulation of the six-phase inverter-start IM was carried in ANSYS electronics desktop software which is based on Maxwell's Equations and the voltage equations of the machine.

2.1. Voltage Equations of The Six-Phase Inverter-Start IM

The voltage equations portray the electrical behaviour of the six-phase inverter start IM. The stator six-phase voltage equations are presented in Equations (1) – (6). Figure 1 depicts the motor stator windings as well as

the set of three rotor phase windings and phasors. The fictitious d-q axis of the six phase IM is as seen in Figure 1. The stator phases are represented as upper case alphabets with subscripts *s*, while the rotor phases are lower case alphabets with subscripts *r*. A dynamic model for a motor with a three-phase rotor winding and a six-phase stator winding is been developed with the stator and rotor voltage equations in Equations (1) – (13).

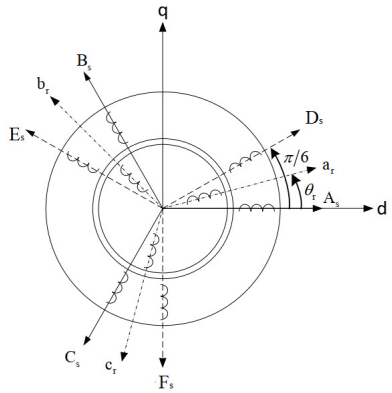

Figure 1: Six-phase induction motor stator and rotor phasors

$$V_{As} = R_{As}i_{As} + \frac{d}{dt}\lambda_{As} \tag{1}$$

$$V_{Bs} = R_{Bs}i_{Bs} + \frac{d}{dt}\lambda_{Bs} \tag{2}$$

$$V_{Cs} = R_{Cs}i_{Cs} + \frac{d}{dt}\lambda_{Cs} \tag{3}$$

$$V_{Ds} = R_{Ds}i_{Ds} + \frac{d}{dt}\lambda_{Ds} \tag{4}$$

$$V_{Es} = R_{Es}i_{Es} + \frac{d}{dt}\lambda_{Es} \tag{5}$$

$$V_{Fs} = R_{Fs}i_{Fs} + \frac{d}{dt}\lambda_{Fs} \tag{6}$$

The rotor voltage equations in Direct-Phase variables are also presented in Equations (7) – (9).

$$V_{ar} = R_{ar}i_{ar} + \frac{d}{dt}\lambda_{ar} \tag{7}$$

$$V_{br} = R_{br}i_{br} + \frac{d}{dt}\lambda_{br} \tag{8}$$

$$V_{cr} = R_{cr}i_{cr} + \frac{d}{dt}\lambda_{cr} \tag{9}$$

where V_{As} = stator phase A voltage, V_{ar} = rotor phase A voltage, R = resistance, i = current and λ = flux linkage.

$$T_{abc\rightarrow dq0} = \begin{bmatrix} cos\,\theta & cos(\theta - \frac{2\pi}{3}) & \cos(\theta - \frac{4\pi}{3}) \\ sin\,\theta & sin(\theta - \frac{2\pi}{3}) & sin(\theta - \frac{4\pi}{3}) \\ \frac{1}{2} & \frac{1}{2} & \frac{1}{2} \end{bmatrix} \tag{10}$$

$$V_{dq}^{r} = [T]V_{abcs} \tag{11}$$

The transformation from direct-phase variables to d-q variables is done using the transformation matrix presented in Equation (10). Equation (11) shows the relationship between the d-q voltages in rotor reference

frame and the stator phase voltages. The electromagnetic torque of the machine is presented in the mechanical model of the machine as seen in Equation (12).

$$T_e = J\left(\frac{2}{P}\right)p\omega_r + T_L \tag{12}$$

where T_L = load torque, J = inertia, P = number of poles, ω_r = rotor speed, and p = differential operator.

2.2. Finite Element Analysis Equations

The finite element method (FEM) is a numerical technique that breaks a large problem space down into smaller spaces known as finite elements, through the use of meshes. The FEA mesh plot is shown in Figure 2. Using FEA in the analysis of electrical machines, the electric and magnetic fields of the machines are determined (Bianchi, 2017). The electric and magnetic vector fields are computed using Maxwell's field equations as presented in Equations (13) – (16).

$$\text{curl}\, H = J + \frac{\partial D}{\partial t} \tag{13}$$

$$\text{curl}\, E = -\frac{\partial B}{\partial t} \tag{14}$$

$$\text{div}\, B = 0 \tag{15}$$

$$\text{div}\, D = \rho \tag{16}$$

Where H = magnetic field strength, J = current density, D = electric field displacement, B = magnetic flux density, E = Maxwell's electric field, and ρ = density of electric charge.

The vector fields in Equations (17) – (20) varies in position and time. The constitutive relationship is presented in Equations (17) – (19) alongside the continuity equation of the vector field in Equation (20).

$$B = \mu H \tag{17}$$

$$D = \epsilon E \tag{18}$$

$$J = \sigma E \tag{19}$$

$$\text{div}\, J = -\frac{\partial \rho}{\partial t} \tag{20}$$

Where σ = electric conductivity, ϵ = electric permittivity, and μ = magnetic permeability.

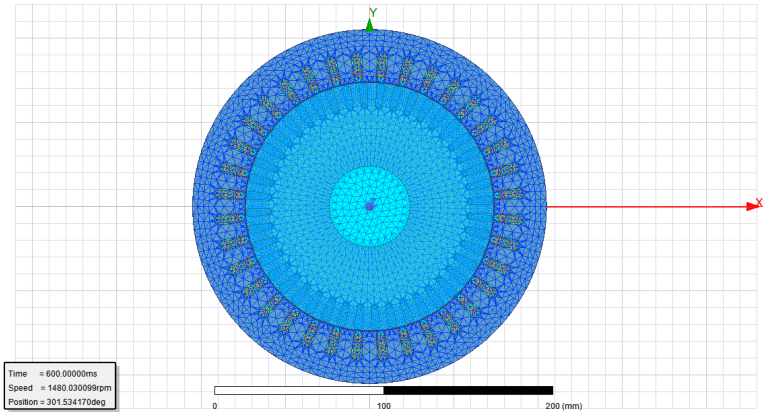

Figure 2: FEA Mesh plot of the six-phase inverter-start IM

In the case of a non-linear material, the coefficients become a function of the magnetic field or electric field, hence magnetic permeability μ becomes a function of H, accounting for saturation, whereas σ and ϵ become functions of Maxwell's electric field E.

Boundary conditions are necessary for determining a solution of the geometry using FEM, as they define the value of the magnetic vector potential on the boundaries of the geometry. There are two typical boundary conditions; Neumann's condition and Dirichlet's condition explained in (Bianchi, 2017). The choice of an appropriate boundary condition gives an excellent result of the machine model.

2.3. Machine Description

The winding clock diagram of the six-phase inverter-start IM model used in this study is presented in Figure 3. The machine model was derived from the conventional three-phase IM, having a single stator winding. The single stator winding was split into two sets of stator windings forming a six-phase machine (Schiferl and Ong, 1983). The six phases were supplied voltages directly from the inverter circuit presented in Figure 4. The various machine parameters and dimensions of the IM used for the FEA simulations were presented in Table 1.

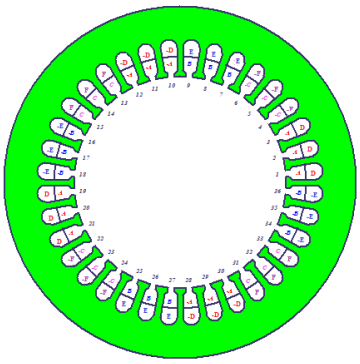

Figure 3: Winding-clock diagram of the six-phase induction motor stator

Table 1: FEA machine design parameters

Machine parameter/configuration	Value
Stator outer diameter	210 mm
Stator inner diameter	148 mm
Rotor outer diameter	147.3 mm
Rotor inner diameter	48 mm
Machine length	250 mm
Stacking factor	0.95
Stator/Rotor steel type	M19_24G
Number of poles	4
Number of slots	36
Conductors per slot	24
Coil pitch	5
Winding layout	Double-layer
Winding type	Whole-coiled
Parallel branch	2
No. of rotor slots	44
Rated voltage	380 V
Rated speed	1500 rpm
Rated output power	7.5 kW

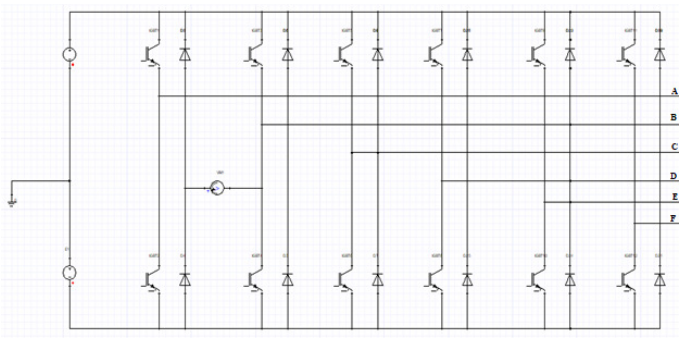

Figure 4: Six-phase voltage source inverter circuit

2.4. Simulation of Six-phase Inverter-Start Induction Motor in d-q variables using MATLAB/Simulink

The simulation of the six-phase inverter-start IM was carried out in MATLAB/Simulink in d-q variables, similar to what was done by Ogunjuyigbe *et al.* (2014). Equations (1) – (13) and some of the machine parameters presented in Table 1 were used for the modelling of the machine. A six-phase PWM inverter circuit was used to achieve the voltage source. It should be noted that the dynamic modelling and simulation was done in per-unit. The IM model was started on no-load and at a time of 1s, a step load of 5 p.u was applied to the motor. Performance characteristics such as speed, torque, stator currents, and torque-speed characteristics were observed and presented in the results section.

2.5. Simulation of Six-phase Inverter-Start Induction Motor using FEA

More detailed machine parameters as presented in Table 1 were required for finite element analysis simulations. Parameters such as stator dimensions, coil sizes, the dimension of slots, number of turns of coils, types of materials employed in the machine, nature of rotor etc. were used for the modelling in ANSYS electronics desktop software. The modelling procedure involved the following steps shown in Figure 5.

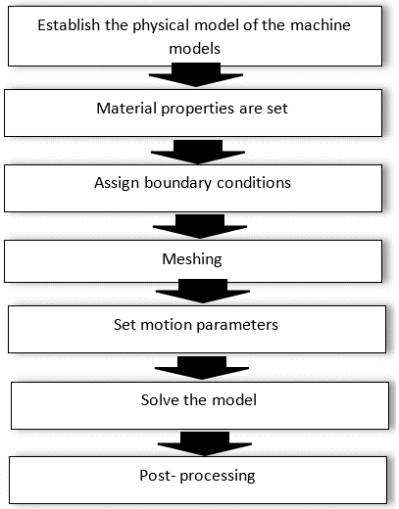

Figure 5: ANSYS FEA software modelling procedure

The six-phase IM was modelled initially using RMxprt software which is a template-based electrical machine design tool in the ANSYS electronics desktop using the dimensions and parameters in Table 1. The six-phase inverter circuit was modelled in ANSYS Twin Builder, while the motor was created in ANSYS

Maxwell 2D environment from the RMxprt model. Figure 6 shows the co-simulation of the voltage source inverter and the designed motor.

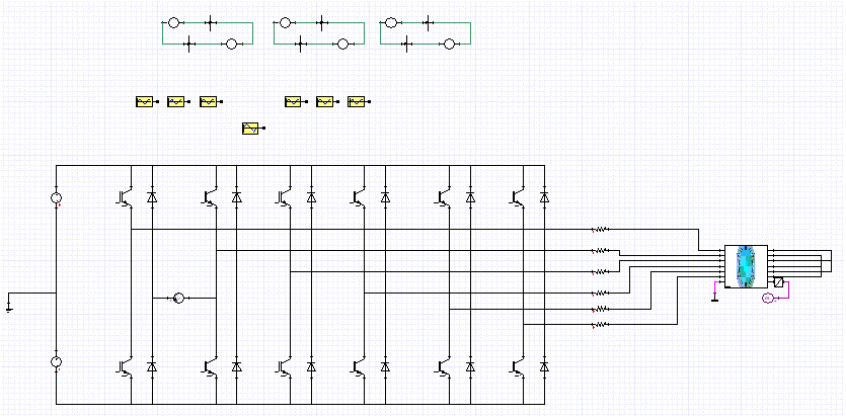

Figure 6: ANSYS FEA co-simulation between ANSYS Twin Builder and ANSYS Maxwell 2D

The voltage source inverter was used to obtain the six-phase supply from the AC supply from an initial 415 V three-phase AC source that was rectified. The initial per-phase AC voltage supply before rectification was 230V. The rectified voltage was fed to the voltage source inverter which was coupled with the six-phase wound IM in ANSYS Maxwell 2D. The IM model was started on no-load and at a time of 0.4 s, a step load of 15 Nm was applied to the motor. Performance parameters such as speed, torque, stator currents, electrical and mechanical powers, magnetic flux density etc., were observed and presented in the results section.

3. RESULTS AND DISCUSSION

The speed characteristics of the six-phase inverter start IM models in d-q and FEA are presented in Figures 7 and 8. The d-q speed plot had an initial transient speed rise of 1510 rpm later settling at a steady-state speed of 1490 rpm at about 0.2 s. At the introduction of a load torque of 5 p.u, the speed dropped to 1380 rpm and later achieved steady-state at 1398 rpm. Similarly, the FEA speed plot showed an initial rise in the speed of 1518 rpm and later settling at 1496 rpm. At the introduction of 15 Nm step load after 0.4 s of simulation, the model was seen to experience transient disturbance before attaining steady-state again at about 1497 rpm.

The torque performance characteristics of the six-phase inverter start IM model in d-q and FEA were presented in Figures 9 and 10. An initial transient torque rise of 19.88 p.u was observed for the d-q model, which later settled at zero when the machine achieved steady-state at 0.2 s. At the introduction of 5 p.u load torque after 1 s, the torque rose to 6.03 p.u and later settled at 5 p.u. For the FEA plot, the motor showed a starting transient rise of 402 Nm, and the machine settled after 0.145 s. The plot showed torque pulsations as a result of magneto-motive force (MMF) permeance and slot harmonics which is not seen in the d-q plot in Figure 9. This is because the FEA considered all the harmonics and also the actual airgap which is not considered in the d-q method. A torque rise was also noticed at the introduction of 25 Nm load torque after 0.4 s, which later settled at 25.01 Nm as seen in Figure 10. The FEA torque plot depicts the actual behavior of the motor on starting and at the introduction of load torque.

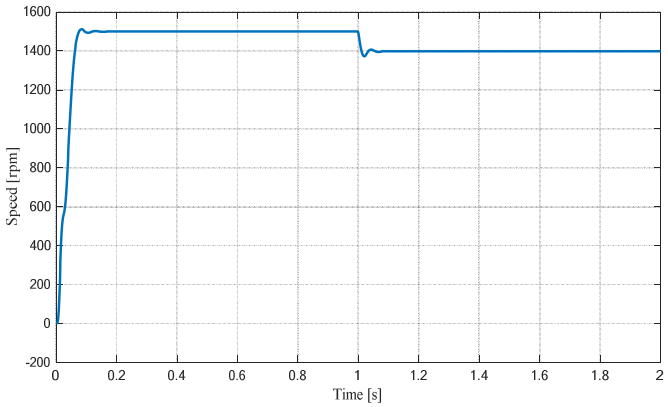

Figure 7: Six-phase inverter-start IM speed characteristic in d-q variables

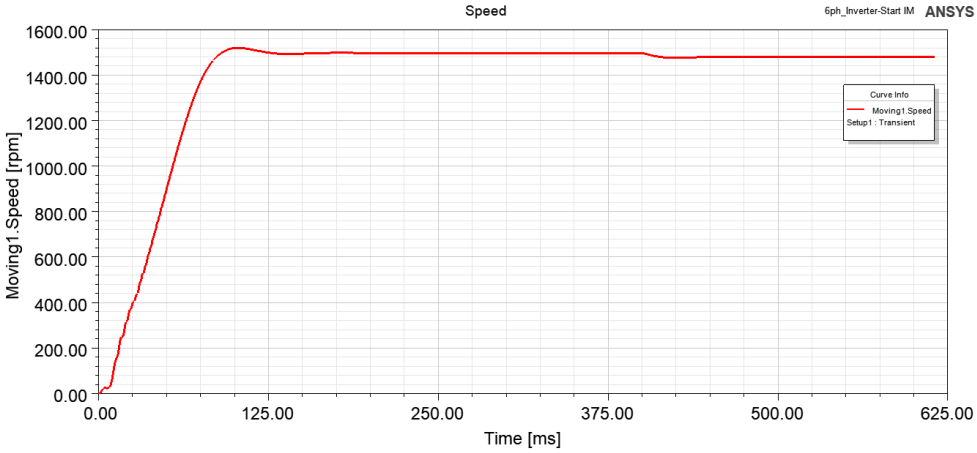

Figure 8: FEA Six-phase inverter-start IM speed characteristic

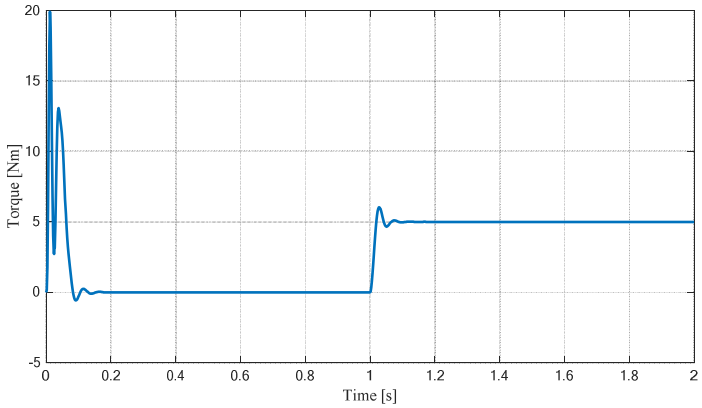

Figure 9: Six-phase inverter-start IM torque characteristic in d-q variables

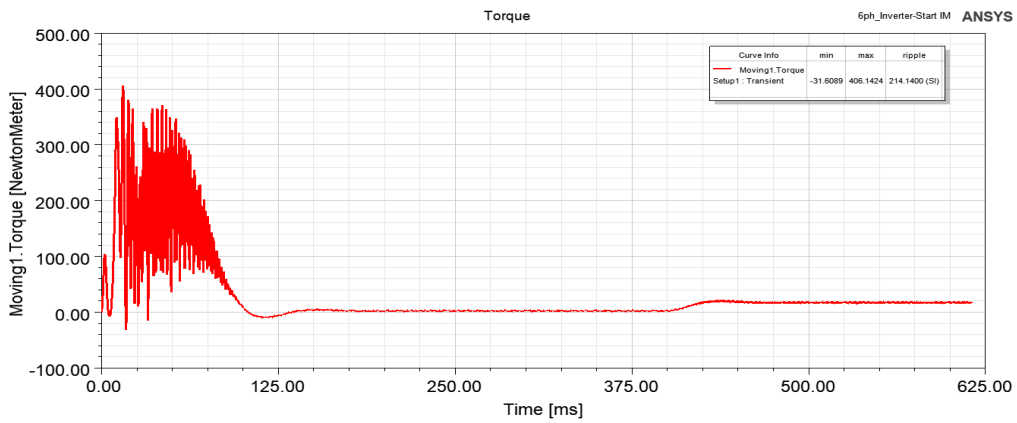

Figure 10: FEA Six-phase inverter-start IM torque characteristic

The stator phase winding currents of the six-phase inverter start IM model in d-q and FEA were shown in Figures 11 and 12. The plots are similar and showed the transient currents rise at start-up and the current rise at the introduction of load torque. The stator phase A current of the motor was observed as 59.35 A (rms), stator phase B had a stator phase current of 59.65 A (rms), phase C had 61.27 A (rms), phase D - 60.37 A (rms), phase E – 61.04 A (rms) and phase F - 61.25 A (rms) in Figure 12.

The torque-speed characteristics of the d-q motor model is presented in Figure 13, while that of the FEA is presented in Figure 14. The torque-speed characteristics illustrate the relationship between the speed and torque of the machine model during the operation stages, from start to full load speed. The d-q torque-speed plot in Figure 13 showed an initial settling torque value of zero at synchronous speed and 5 p.u at the introduction of load. The FEA torque-speed plot in Figure 14 demonstrated that an initial settling torque value of 0 Nm was obtained at synchronous speed. When a load is applied, the torque value rises from 0 Nm to a settling value of 25 Nm, indicating full load torque at full load speed. It was also observed from the torque-speed plots that the FEA had torque pulsations due to spatial harmonics while the d-q plot does not show this phenomenom.

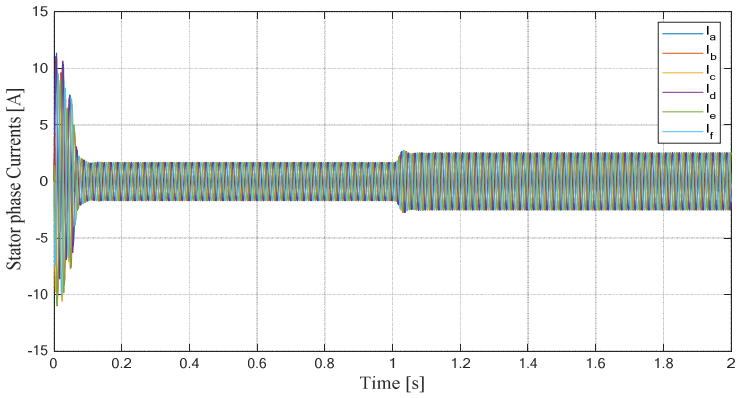

Figure 11: Six-phase inverter-start IM stator phase currents in d-q variables

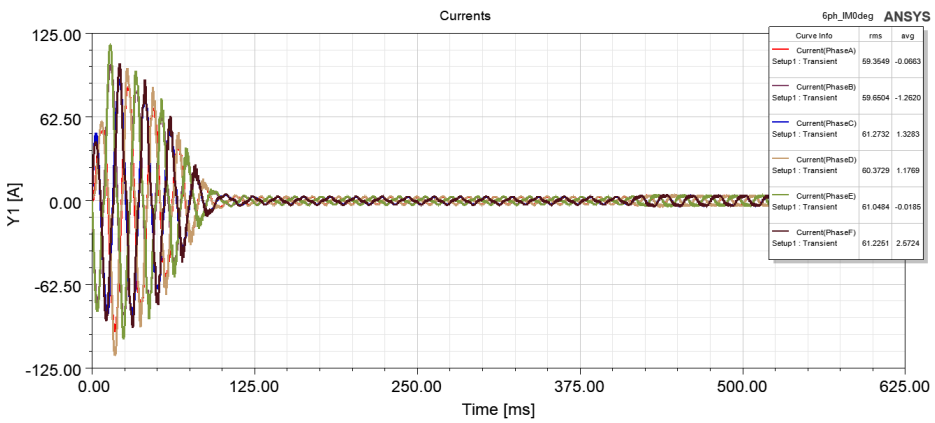

Figure 12: FEA Six-phase inverter-start IM stator phase currents

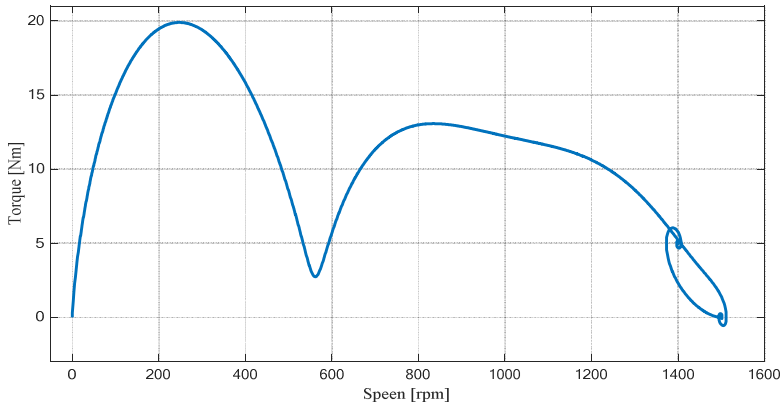

Figure 13: Six-phase inverter-start IM torque-speed characteristic in d-q variables

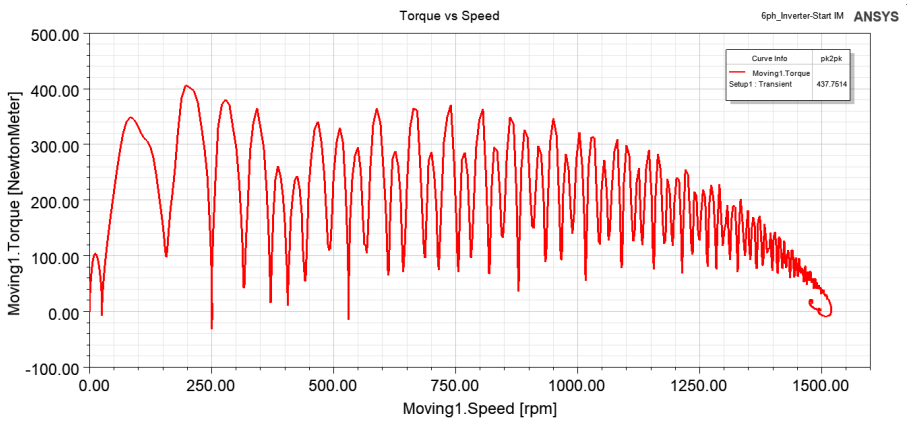

Figure 14: Six-phase inverter-start IM torque-speed characteristic

The FEA model of the electrical and mechanical power developed was presented in Figures 15 and 16. For brevity, the electrical and mechanical power developed for the d-q model was not presented. The average electrical power developed was 24679.58 W. The effects from the addition of 15 Nm load torque after 0.4 s was clearly seen in the mechanical and electrical power plots.

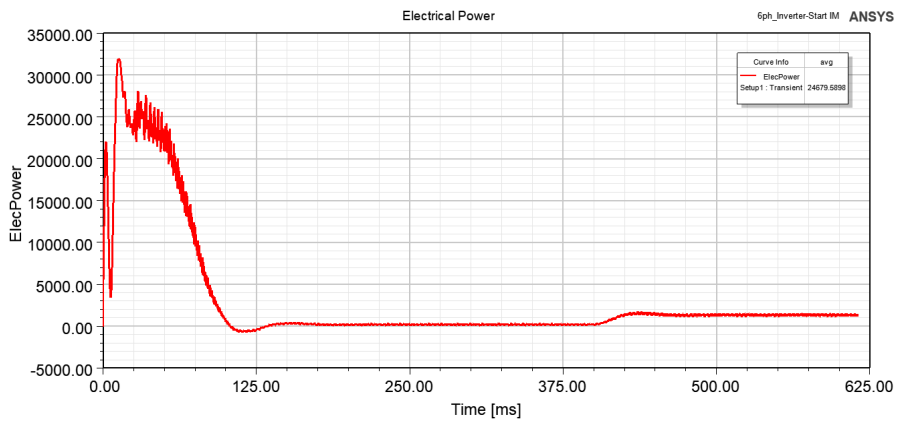

Figure 15: Six-phase inverter-start IM electrical power plot

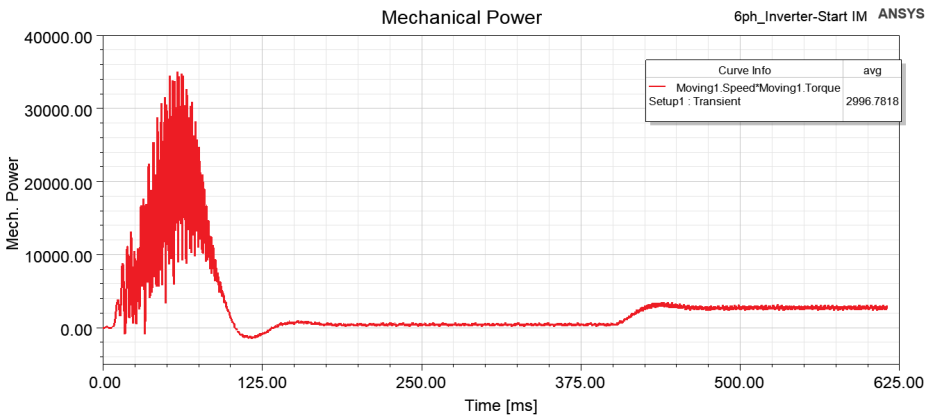

Figure 16: Six-phase inverter-start IM mechanical power plot

The field results of the six-phase inverter-start IM were shown in Figures 17 and 18. The magnetic vector potential of the machine model presented in Figure 17 had a maximum magnetic vector potential value of 0.0189 Wb/m, and minimum magnetic vector potential of -0.0.189 Wb/m. The magnetic flux density of the model presented in Figure 18 had a maximum magnetic flux density of 1.59 T and a minimum magnetic flux density value of 7.12×10^{-7} T. These plots were derived in ANSYS using the earlier presented Maxwell's Equations in (14) – (20). The plot obviously cannot be achieved in MATLAB/Simulink with the conventional d-q method. The magnetic flux densities and magnetic flux lines distributions of the six-phase inverter-start IM are clearly visible in the plots.

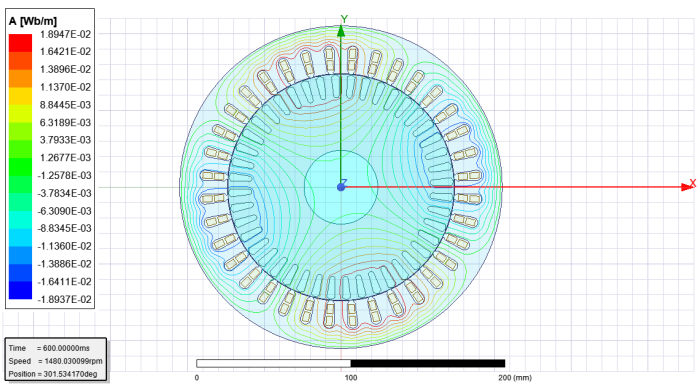

Figure 17: Six-phase inverter-start IM magnetic flux lines showing the magnetic vector potential

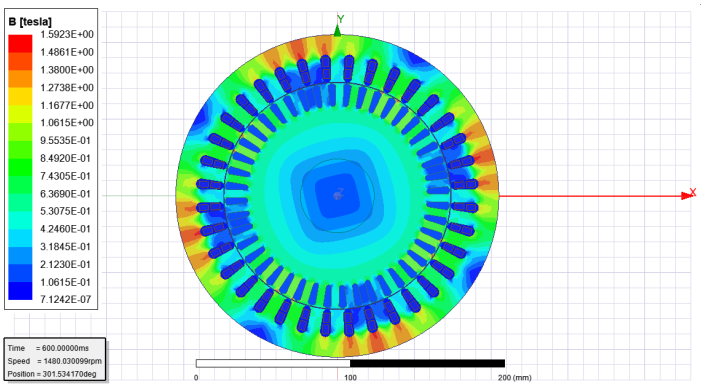

Figure 18: Six-phase inverter-start IM magnetic flux density magnitude

4. CONCLUSION

This paper showed the step-by-step modelling and simulation of a six-phase inverter-start induction motor using the transient co-simulation procedure of ANSYS Maxwell 2D® software and ANSYS Twin Builder software. The study also presented the conventional d-q method in MATLAB/Simulink for comparison. The starting transient and dynamic response at the introduction of load torque of both models were presented in the study. The study showed the possibility of modelling and analyzing inverter-start motors in ANSYS Electronics Desktop Suite and the fact that FEA remains the most accurate method for analyzing electrical machines since the machine parameters are accurately calculated through the direct evaluation of the magnetic field in the machine domain. The ANSYS simulation provided an actual and accurate insight into the operation of the six-phase inverter start motor that other numerical methods cannot provide.

5. ACKNOWLEDGMENT

The authors acknowledge the financial support received from the Petroleum Technology Development Fund (PTDF) under scholar no. PTDF/ED/LSS/PHD/AME/142/17.

6. CONFLICT OF INTEREST

There is no conflict of interest associated with this work.

REFERENCES

Abbas, M. A., Christen, R. and Jahns, T. M. (1984). Six-phase voltage source inverter driven induction motor. *IEEE Transactions on industry applications*, (5), pp. 1251-1259.

Bianchi, N. (2017). *Electrical machine analysis using finite elements*. CRC press.

Dattu, N. A. and Rashmi, M. R. (2017, December). Modelling of five-phase induction motor drive. In: Proceedings of the *2017 International Conference on Technological Advancements in Power and Energy (TAP Energy) December 21-23 2017, Kollam, India,* pp. 1-5.

De Rossiter Correa, M. B., Jacobina, C. B., Da Silva, E. C. and Lima, A. N. (2001). An induction motor drive system with improved fault tolerance. *IEEE Transactions on Industry Applications*, *37*(3), pp. 873-879.

Epemu, A., Obe, P. and Obe, E. (2021). Modelling and analysis of concentrated and distributed winding synchronous reluctance motors in direct-phase variables and finite element analysis. Przeglad Elektrotechniczny, 97(10), pp. 69–75.

Gaikwad, S. A. and Shinde, S. M. (2020, February). Review on Five-phase Induction Motor fed by Five-phase Voltage Source Inverter with different Conduction Mode. In: Proceedings of the *2020 International Conference on Industry 4.0 Technology (I4Tech)* February 13-15 2020, Pune, India. pp. 199-202.

Ghani, S. N. (1988). Digital computer simulation of three-phase induction machine dynamics-a generalized approach. *IEEE transactions on industry applications*, *24*(1), pp. 106-114.

Kaliyavarathan, S. and Sivakumaran, T. S. (2020). Design and performance analysis of novel multiphase induction motor with die-cast copper rotors using FEA for electric propulsion vehicles applications. *Circuit World, 46*(4), pp. 271-280.

Kammoun, J. K., Hadj, N. B. and Ghariani, M. (2015). Induction Motor Finite Element Analysis for EV Application, Torque Ripple and Inter-turn circuit. *Journal of Electrical Systems*, *11*(4), pp 447-462.

Khoucha, F., Lagoun, S. M., Marouani, K., Kheloui, A. and Benbouzid, M. E. H. (2009). Hybrid cascaded H-bridge multilevel-inverter induction-motor-drive direct torque control for automotive applications. *IEEE Transactions on Industrial Electronics*, *57*(3), pp. 892-899.

Krause, P. C. and Thomas, C. H. (1965). Simulation of symmetrical induction machinery. *IEEE transactions on power apparatus and systems*, *84*(11), pp. 1038-1053.

Kundrotas, B., Lisauskas, S. and Rinkeviciene, R. (2011). Model of multiphase induction motor. *Elektronika ir Elektrotechnika*, *111*(5), pp. 111-114.

Levi, E., Bojoi, R., Profumo, F., Toliyat, H. A. and Williamson, S. (2007). Multiphase induction motor drives-a technology status review. *IET Electric Power Applications*, *1*(4), pp. 489-516.

Liang, X. and Ilochonwu, O. (2010). Induction motor starting in practical industrial applications. *IEEE Transactions on Industry Applications, 47*(1), 271-280.

Melfi, M. J., Evon, S. and McElveen, R. (2009). Induction versus permanent magnet motors. *IEEE Industry Applications Magazine, 15*(6), 28-35.

Ogunjuyigbe, A. S. O., Nnachi, A., Jimoh, A. and Nicolae, D. (2014). Simulation of Six phase Induction machine split winding Induction Machine using MATLAB / SIMULINK environment. *Journal of Electrical Engineering, 8*(3), pp. 33-39.

Schiferl, R. F. and Ong, C. M. (1983). Six phase synchronous machine with AC and DC stator connections, Part I: Equivalent circuit representation and steady-state analysis. *IEEE Transactions on Power Apparatus and Systems*, (8), pp. 2685-2693.

Singh, G. K., Pant, V. and Singh, Y. P. (2003). Voltage source inverter driven multi-phase induction machine. *Computers & Electrical Engineering*, *29*(8), pp. 813-834.

Loriya, V. J. and Patel, R. A. (2016). Performance Analysis of Five-Phase and Three-Phase Induction Machines. *International Journal of Innovative Research in Electrical, Electronic, Instrumentation and Control Engineering*, *4*(1), pp. 77-82.

Ward, E. E. and Härer, H. (1969). Preliminary investigation of an inverter-fed 5-phase induction motor. In *Proceedings of the Institution of Electrical Engineers* 116(6), pp. 980-984.